

Electrochemical and Photoelectrochemical Properties of Nano-Islands of Zinc and Niobium Oxides Deposited on Aluminum Thin Film by RF Magnetron Reactive Sputtering

Go Sajiki^{1*}, Yasuhiko Benino², Tokuro Nanba², Hiroshi Okano³

¹Technological, Educational Supporting Center in Takamatsu, Kagawa National College of Technology, Takamatsu, Japan

²Graduate School of Environmental and Life Science, Okayama University, Okayama, Japan

³General Education, Kagawa National College of Technology, Takamatsu, Japan

Email: * sajiki@t.kagawa-nct.ac.jp

Received 17 February 2015; accepted 6 April 2015; published 8 April 2015

Copyright © 2015 by authors and Scientific Research Publishing Inc.

This work is licensed under the Creative Commons Attribution International License (CC BY).

<http://creativecommons.org/licenses/by/4.0/>



Open Access

Abstract

Zinc oxide (ZnO) and niobium oxide (NbO_x) with a nano-island structure were deposited by a sputtering method on Al-coated glass substrates. Cells with a (ZnO or NbO_x)/Al/glass|KNO₃aq.|Al/glass structure were assembled, and electrochemical and photoelectrochemical properties were evaluated. The ZnO and NbO_x electrodes had higher electrode potentials than the counter Al/glass electrode, and electron flows from the counter electrode to the ZnO and NbO_x electrodes through the external circuit were commonly confirmed. In the ZnO-based cell, only faint photocurrent generation was seen, where Zn and Al elution from the ZnO electrode was found. In the NbO_x-based cell, however, stable generation of electricity was successfully achieved, and electrode corrosion was not recognized even in microscopic observations. A photoelectrochemical conversion model was proposed based on potential-pH diagrams. In the case of nano-island structures formed at shorter NbO_x deposition time, it was concluded that the photoelectrochemical reactions, which were proceeded in the immediate vicinity of the boundary among nano-islands, substrate, and electrolyte solution, were predominant for the photoelectrochemical conversion, and in the case of film structures with longer deposition time, the predominant reactions took place at the film surface.

*Corresponding author.

Keywords

Nano-Island, Electrochemistry, Photoelectrochemistry, Niobium and Zinc Oxide, Corrosion

1. Introduction

In recent years, various energy conversion devices, such as photovoltaic, thermoelectric, and piezoelectric devices, have been extensively studied because fossil fuel may run out within the next several decades. Among the devices, it is guessed that demand for the photovoltaic solar cells rises rapidly, because solar energy is semipermanent and is used anywhere under sunlight. However, there are various problems in solar cells, such as material cost, process cost, and power generation efficiency, and a number of attempts have been made to solve these problems [1]-[5]. Photoelectrochemical cells (PECs) have been also studied extensively [6]-[10], because they can produce not only electricity but also chemical energies such as hydrogen and oxygen by water splitting [11].

In the authors' research group [12], a laminated structure of ZnO (nano-islands)/Al (thin film)/glass was prepared, and it was found that Al thin film was etched in deionized water under UV irradiation by photocatalytic effect of ZnO nano-islands [12]. It was supposed that the Al-etching was due to an oxidation-reduction reaction, and hence if a cell had been formed, it should have been a solar cell. Then, in the present study, photoelectrochemical property of ZnO nano-islands was evaluated by using the ZnO/Al/glass structure as a photovoltaic electrode. In the previous study [12], Al elution from the electrode was observed, which was not suitable for PEC, and the electrodes must be electrochemically stable. Then, electrochemical property was also investigated in the present study. On the other hand, it was reported that Nb₂O₅ had photocatalytic activity and showed higher deterioration resistance in photocatalytic activity than ZnO [13]. Hence, in the present study, NbO_x nano-islands were also deposited on the Al/glass substrate for expecting higher corrosion and acid resistance than ZnO, and electrochemical and photoelectrochemical properties were examined.

Anyway, PECs have not been put to practical use yet, because the conversion efficiency had been not enough. In order to improve the conversion efficiency, various nano-textures have been studied so far: for example in ZnO and NbO_x, nanotubes [14] [15], nanowires [16] [17], nanoparticles [18] [19], nanorods [20] [21] and so on [22]-[26]. To the best of the authors' knowledge, PECs with a nano-island structure have never been reported, where nano-islands are two-dimensionally and separately distributed on a substrate, and they are not in a stacking structure with nano-particles.

In the present study, not only nano-island but also continuous film structures of NbO_x deposits were fabricated by changing deposition time to clarify the nano-texture dependence on the electrochemical and photoelectrochemical properties, in which surface states of ZnO and NbO_x/Al/glass electrodes and Al/glass substrate were observed by atomic force microscopy (AFM), and valence states of niobium ions were also investigated by optical absorption measurement. The electrochemical and photoelectrochemical reactions in the ZnO- and NbO_x-based PECs were discussed based on the experimental results.

2. Experiment

2.1. Fabrication of Photovoltaic Electrodes

Al thin films were deposited on a glass (SCHOTT Nippon K.K., Glass code: D263T) substrate by a radio frequency (RF) magnetron sputtering (SHINKO SEIKI CO., LTD, Type: SRV4320), where the deposition time was extended to 40 min, obtaining 100 nm of Al films. The Al-coated glass substrate was also used as a counter electrode of PEC. ZnO or NbO_x was deposited on the Al/glass substrate by RF magnetron reactive sputtering (ULVAC JAPAN, Ltd., Model: YH-500A or DIAVAC LIMITED, Type: DS-412Z, respectively). **Figure 1** shows the structure of ZnO or NbO_x/Al/glass photovoltaic electrode. **Table 1** shows the deposition conditions of Al, ZnO and NbO_x, respectively.

2.2. Electrochemical and Photoelectrochemical Measurements

Figure 2 shows the schematic of PEC used in photoelectrochemical measurements. KNO₃ solution was commonly used as an electrolyte solution in both the electrochemical and photoelectrochemical measurements.

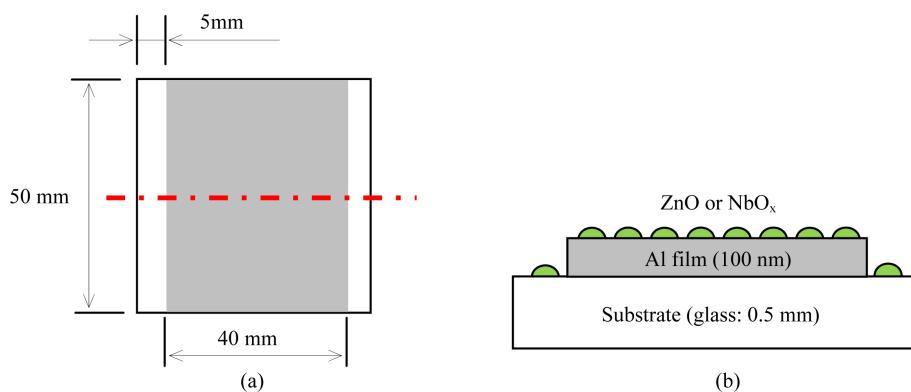


Figure 1. Schematic of photovoltaic electrode: (a) top view and (b) cross section.

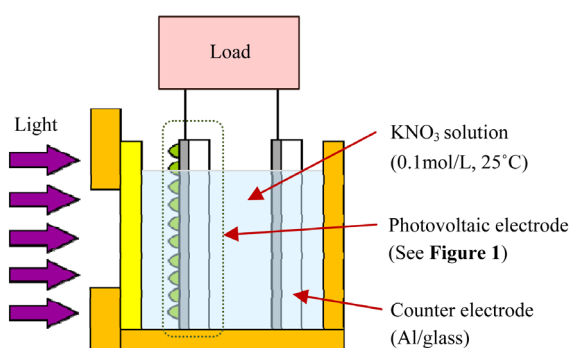


Figure 2. Schematic of PEC used in photoelectrochemical measurements.

Table 1. Deposition conditions of Al, ZnO and NbO_x by RF magnetron sputtering.

	Al	ZnO	NbO _x
Substrate	Glass	Al/glass	Al/glass, quartz glass
Target	ϕ101.6 mm, Al (99.9%)	ϕ50 mm, Zn (99.99%)	ϕ50 mm, Nb (99.99%)
Ar gas	99.99%, 1.0 ccm	99.99%, 1.8 ccm	99.99%, 6.0 ccm
O ₂ gas	-	99.99%, 2.4 ccm	99.99%, 6.0 ccm
Orbital speed of substrate holders	1800 rpm	-	-
Distance from substrate to target	100 mm	60 mm	60 mm
RF power, and frequency	50 W, 13.56 MHz	200 W, 13.56 MHz	200 W, 13.56 MHz
Back pressure	$<8.0 \times 10^{-5}$ Pa	$<6.7 \times 10^{-4}$ Pa	$<6.7 \times 10^{-4}$ Pa
Deposition pressure	9.3×10^{-2} Pa	0.39 Pa	0.39 Pa
Deposition rate	0.042 nm/s	1 nm/s	0.17 nm/s
Deposition time	2400 s	3, 17 s	10 - 300 s

KNO₃ was dissolved in a distilled water (Wako Pure Chemical Industries, Ltd., CAS No.: 7732-18-5, 200 ml), obtaining 0.1 mol/L electrolyte solution. During the measurements, the electrolyte solution was kept at a constant temperature of 25°C, and the measurements were done in a dark place.

Firstly, the electrode potential was measured. The ZnO or NbO_x/Al/glass electrode and a carbon counter electrode (NaRiKa Corporation, CAT. NO. B10-2050-09) were immersed in the electrolyte solution. The electrodes

were connected to a potentiostat (Bio Logic, SP-50), and an Ag/AgCl electrode in saturated KCl solution (HOKUTO DENKO Co., HX-R6) was also connected as a reference electrode. The potential of the electrodes with respect to the reference electrode was determined by measuring open circuit voltage for 100 s. Subsequently, electrochemical stability, that is, corrosion resistance of the electrodes was evaluated, where a constant load discharge (CLD) mode with an electrical resistance of 100 k Ω installed in the potentiostat was used. At this time, Al/glass soaked in a separate beaker was used as a counter electrode, and the beakers were connected with a KNO₃ salt bridge. Elution of Nb, Zn and Al in the electrodes was investigated after immersing the electrodes for 1 hour. Inductively coupled plasma measurement (SEIKO and VARIAN Inst., Vista-PRO CCD Simultaneous ICP-OES) was used for the detection of the elements eluted in the electrolyte solution.

In the evaluation of photoelectrochemical properties, photocurrent generation was firstly measured by using the PEC shown in **Figure 2**, where a solar simulator (SAN-EI ELECTRIC, XES-40S1, Irradiance: 1000 W/m²) was used as a light source. The CLD mode with 100 k Ω resistance installed in the potentiostat apparatus was also used in the photocurrent measurements. During the measurements, voltage was not controlled by the potentiostat, and only the current passing through the resistance in the potentiostat apparatus was measured. The ZnO or NbO_x side of the photovoltaic electrodes was exposed to a simulated sunlight generated by the solar simulator. The power supply of the potentiostat was turned on. After waiting for 100 s without irradiation, the light emitted from the solar simulator was irradiated to the photovoltaic electrode for 300 s. The irradiation was repeated for 9 times at an interval of 100 s, and the total measurement time was 3600 s. After the measurements, elution of the electrode constituents was also evaluated by ICP.

Finally, electricity generation property was investigated by measuring current and voltage generated by the light irradiation. In the measurement, the cell setup given in **Figure 2** was also used, and a variable resistor (YOKOGAWA ELECTRO WORKS. LTD., Decade Resistance Box Type 2793, Max: 111.1110 M Ω) was, however, connected to the electrodes instead of the constant load. The current and voltage were measured by using multimeters (Agilent Technologies, Inc., Agilent 34,450 A 5 1/2 Digit Multimeter). Photocurrent and photovoltage were measured by changing resistance. Dark current and voltage measurement without light irradiation was also carried out, and net electricity generation was evaluated by subtracting dark current and voltage from photocurrent and photovoltage.

2.3. Surface Observation by AFM

In the previous report [12], ZnO nano-islands were not distinguished clearly by AFM (Bruker AXS K.K., Dimension Icon). In the present study, a tapping mode AFM apparatus was also used, where a phase mode was applied to distinguish the NbO_x or ZnO deposits from the Al thin film. In the phase mode, the difference in hardness of two substances, that is, metal and oxide, appears in the difference in phase angle, which can be used for the distinction.

2.4. Measurement of Optical States

In the previous study [12], X-ray diffraction (XRD) measurement (Rigaku Corporation, Ultima IV) indicated that ZnO deposits were crystalline. However, it was guessed that NbO_x deposits were amorphous [27], and actually sharp peaks were not observed in XRD patterns. It is generally known that band gap of Nb₂O₅ is 3.4 eV, and it is hence expected that the stoichiometry of NbO_x is estimated from the optical absorption edge. Then, optical absorption measurement was performed by using a double-beam spectrophotometer method (Shimadzu Corporation, UV-3100). For the measurement, NbO_x were directly deposited on a quartz glass substrate (Sendai quartz glass Works, Co. Ltd., Synthetic quartz glass, SUPRASIL-P30) under the same conditions given in **Table 1**. Furthermore, the absorption spectra for the reagents, NbO (Kojundo Chemical Lab. Co., Ltd., Cat. No. NBO01PB), NbO₂ (NBO02PB), and Nb₂O₅ (NBO06PB) were also measured with an integrating sphere (JASCO Corporation, ISN-470) for comparison.

3. Results

3.1. Electrochemical Property

Electrode potentials are shown in **Table 2**. The electrode potential of Al/glass (−0.70 V vs. Ag/AgCl), which is higher than the standard electrode potential of Al (−1.662 V vs. SHE, standard hydrogen electrode) [28]. The

Table 2. Electrode potentials obtained by open circuit voltage measurement.

Electrode	Deposition time (s)	Electrode potential (V vs. Ag/AgCl)
Al/glass	-	-0.70
ZnO/Al/glass	3	-0.55
	17	-0.46
	10	-0.19
	15	-0.25
	17	-0.19
	20	-0.07
NbO _x /Al/glass	30	-0.04
	40	0.00
	60	0.07
	100	0.11
	150	0.19
	200	0.20
	300	0.23

electrode potentials of ZnO- and NbO_x-deposited electrodes are higher than those of the Al/glass electrodes. In NbO_x/Al/glass electrode, the electrode potential increases with increasing the deposition time, and similar trend is also seen in ZnO/Al/glass electrode. During the potential measurements, the electrode potential of NbO_x-deposited electrodes was stable and almost constant with small fluctuation. In the case of ZnO-deposited electrodes, however, the electrode potential decreased continuously during the measurements, and the electrode with shorter deposition time had higher rate of decrease in electrode potential. The decrease in the electrode potential during the measurements suggests the two possible changes in the ZnO-deposited electrodes, that is, the reduction of Zn from 2+ to 0 in valence number and the dissolution of ZnO deposits into the electrolyte solution.

After electrochemical corrosion tests, the elution of Al and Zn from ZnO/Al/glass electrodes is confirmed, and such the elution is not observed in NbO_x/Al/glass electrodes. The elution is discussed later.

3.2. Photoelectrochemical Property

Figure 3 shows the photocurrent density curves of ZnO- and NbO_x-based PECs. In these PECs, ZnO and NbO_x were deposited for 3, 17 s and 17, 100 s at the apparent deposition rates of 1.00 and 0.17 nm/s, respectively, expecting the comparable thicknesses of ca. 3 and 17 nm. In the previous study [12], it was confirmed that ZnO deposits were present as nano-islands at these thicknesses. As shown in **Figure 3**, current generation during the light irradiation is successfully confirmed in the NbO_x-based PECs, where current generation is stable, and very little degradation is observed in current generation even after repeating irradiation. In case of the ZnO deposits, current decreases rapidly and changes into increase just before irradiation. Even after starting irradiation, current increases slowly and continuously, and in the case of 3 s ZnO-deposited PEC, current stops increasing at ca. 1700 s. Even when light was not irradiated, almost the same current curves were obtained, suggesting that most of current obtained in the ZnO-based PECs was caused not by photoelectrochemical but by electrochemical reactions. However, only in 3 s ZnO-deposited PEC, small but clear decrease in current is recognized after stopping 4th irradiation, which indicates photocurrent generation by photo-induced electrochemical reactions. When the light irradiation is continued for a few hours or more, very small and few bubbles are generated at all the electrodes, that is, photovoltaic and counter electrodes in both NbO_x and ZnO-based PECs.

In the previous study of ZnO nano-islands [12], Al-etching under UV irradiation was observed, and as mentioned, the elution of Zn and Al in ZnO/Al/glass electrode was also confirmed in dark place. **Table 3** shows the concentrations of the elements eluted from ZnO/Al/glass electrodes during the electrochemical corrosion tests

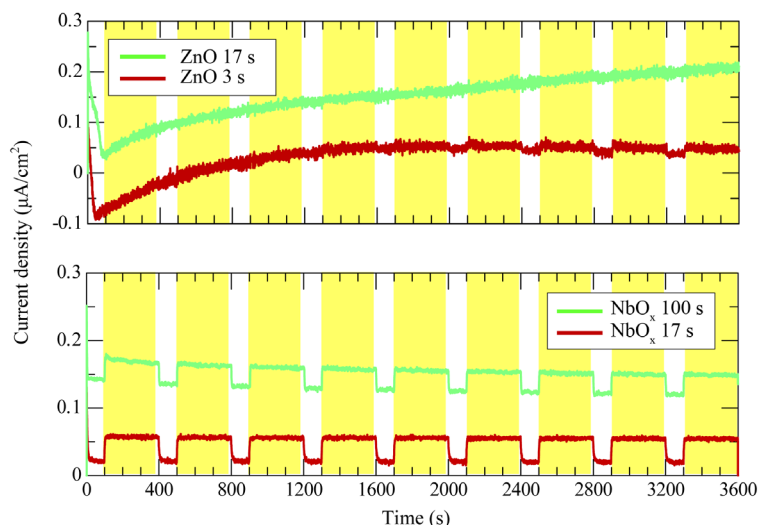


Figure 3. Photocurrent density curves of ZnO and NbO_x-based PECs prepared at different deposition times. Yellow regions show the light irradiating periods.

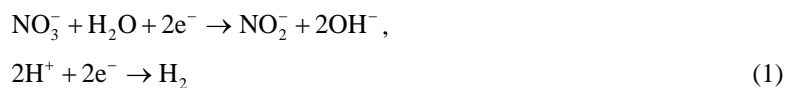
Table 3. Concentrations of the elements eluted from ZnO/Al/glass electrodes during the electrochemical corrosion and photocurrent generation tests obtained by ICP measurement.

Test	ZnO deposition time (s)	Al (ppb)	Zn (ppb)
Corrosion	3	7	72
	17	8	80
Photocurrent generation	3	12	116
	17	28	143

and photocurrent measurements. After the photocurrent measurements, Zn and Al were confirmed in the electrolyte solution, and the concentrations were larger as compared with the case without light irradiation. Therefore, it is supposed that the electrochemical reactions resulting in the elution of Zn and Al are accelerated by their radiation. In case of the NbO_x-based PECs, neither Al nor Nb elution was detected in the photovoltaic electrode. However, Al elution from the counter electrodes was confirmed in both PECs.

In both PECs, electrons flowed from the counter electrode into the photovoltaic electrode through the external circuit during light irradiation. The direction of electron flow was the same even in the electrochemically-unstable ZnO-based PECs. According to the direction of electron flow, following reduction and oxidation reactions are expected at the photovoltaic and counter electrodes, respectively.

Photovoltaic electrode:



Counter electrode:



However, the current flow observed in the present study is opposite to the direction commonly observed in wet-type solar cells with semiconductor electrodes, such as TiO₂ [29]-[31].

Figure 4 shows the relation between photocurrent density, J and photovoltage, V (J - V curve) at different deposition time of NbO_x. By subtracting dark current and dark voltage from photocurrent and photovoltage obtained at the same electrical resistance, the net photocurrent and photovoltage generated by light irradiation were estimated, obtaining the net J - V curve. In general, gradual and steep decreases in photocurrent density at lower and higher photovoltage regions are expected in typical PECs, and in the PECs shown in **Figure 4**, however, an

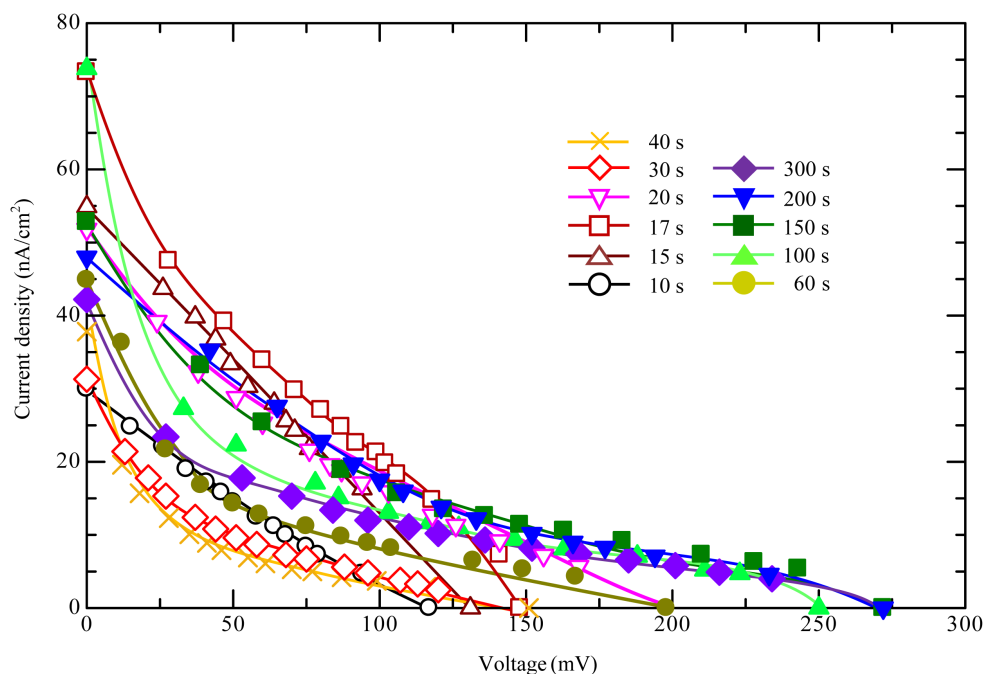


Figure 4. Photocurrent density vs. photovoltage J - V curves measured for the NbO_x -based PECs at different deposition time.

opposite change in J - V curve is commonly observed, that is, steep and gradual decreases in J are seen at lower and higher V regions, respectively.

Then, fill factor, FF is calculated from the equation, $FF = P_{\max}/(J_{\text{sc}} \times V_{\text{oc}})$, where P_{\max} is the maximum power density, J_{sc} is the short circuit current density, and V_{oc} is the open circuit voltage. **Figure 5** shows J_{sc} , V_{oc} , P_{\max} and FF of the NbO_x -based PECs at the different NbO_x deposition time. J_{sc} and P_{\max} reach respective maxima of ca. 100 nA/cm^2 and 2.9 nW/cm^2 at the deposition time of 17 s. FF reaches maximum of ca. 25% at the deposition time of 15 s. V_{oc} reaches maximum of ca. 270 mV at the deposition time of 150 s. J_{sc} and P_{\max} indicate second maxima at the deposition times of 100 and 150 s, respectively. The detail of photoelectrochemical conversion mechanism is discussed later.

3.3. Surface Characterization by AFM

Figure 6 shows the height images (a)-(e) and the phase images (f)-(j) obtained by AFM for the $\text{NbO}_x/\text{Al}/\text{glass}$ electrodes before the photoelectrochemical measurement. Comparing the height images, surface roughness of NbO_x -undeposited Al/glass substrate (**Figure 6(a)**) and NbO_x -deposited $\text{NbO}_x/\text{Al}/\text{glass}$ substrates (**Figures 6(b)-(d)**) at deposition time ≤ 40 s) is almost unchanged. As for the phase images, the NbO_x -undeposited Al/glass substrate indicates the phase angle of ca. 45° (**Figure 6(f)**), which may correspond to oxidized surface layer of Al film. In the NbO_x -deposited specimens (**Figures 6(g)-(j)**), components with the phase angles of -60° and $0^\circ - 45^\circ$ are confirmed. It is thought that these components are metallic Al and NbO_x , respectively, because the $0^\circ - 45^\circ$ component increases with increasing the deposition time. It is supposed that the oxidized surface Al layer (phase angle = 45°) is removed or reduced to metallic state (-60°) by NbO_x sputter deposition. In the phase images, nano-islands of NbO_x deposits are also confirmed at the deposition time of 10 s. The further deposition results in the growth and densification of NbO_x islands at the deposition time of 40 s (**Figure 6(i)**), and the surface of Al/glass substrate is almost completely covered with a film of NbO_x at the deposition time of 100 s (**Figure 6(j)**).

In **Figure 6**, two-dimensional phase images (k-n) are also shown, in which points with the phase angles larger than -20° are shown in white, which indicate NbO_x . At the deposition time ≤ 20 s, growth of NbO_x in an island state is confirmed. At the longer deposition time = 100 s, NbO_x are in a film state, and the underlying Al/glass substrate seems like lakes. Surface area of NbO_x increases continuously with increasing the deposition time.

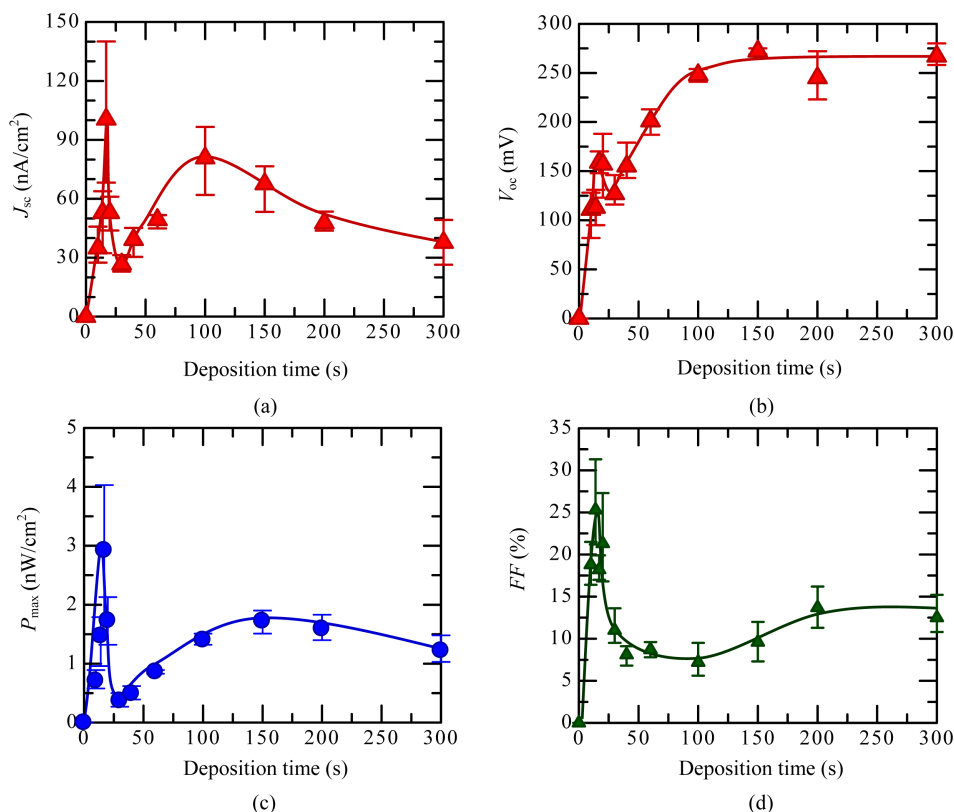


Figure 5. (a) Short circuit current density (J_{sc}), (b) open circuit voltage (V_{oc}), (c) maximum power density (P_{max}), and (d) fill factor (FF) of NbO_x-based PECs prepared at different deposition time.

After the photoelectrochemical measurement (Figure 3), AFM observation was performed again. Figure 7 shows AFM images and two dimensional images of the NbO_x/Al/glass electrode at the NbO_x deposition time of 17 s as-deposited and after 9 repetitions of photo irradiation in the photoelectrochemical measurement. During the repetitions, the electrode was kept in the electrolyte solution without being exposed to the atmosphere. In the AFM images, nano-island structures are confirmed, and quite little change is observed as compared with the as-prepared specimen. On the other hand, in the Al/glass counter electrode (Figure 7(c)), surface roughness increases slightly as compared with the as-deposited one (Figure 6(a)), and the surface with phaseangle of ca. 0° is newly found other than that of 45° (Figure 7(f)). It is probably due to the Al elution. Figure 8 shows the AFM images of the ZnO/Al/glass electrode with the ZnO deposition time of 3 s. In the as-prepared electrode, nano-islands of ZnO deposits are confirmed (Figure 8(d)), and in the electrode after the 1st photoelectrochemical measurement, however, larger islands are also observed in the phase image (Figure 8(e)), and the surface roughness given in Figure 8(b) indicates a small change. The maximum phase angle increases slightly from 50 to 70° in the electrodes before and after the photoelectrochemical measurement, suggesting that the surface is covered with some different substance other than ZnO. After 9 repetitions of the light irradiation, the nano-islands grow higher, and the ditches become deeper, as shown in the height image (Figure 8(c)), and the surface is covered with a substance with large phase angle of 70° (Figure 8(f)). The ditches reach a depth of -16 nm, corresponding to 1/6 of the thickness of Al film (100 nm). As mentioned, Al and Zn elution from ZnO/Al/glass electrodes is confirmed, and it is therefore supposed that Al film and ZnO deposits are eluted in the electrolyte solution, and the eluted Al and Zn species are re-precipitated as solids, probably Al(OH)₃ and Zn(OH)₂, which cover for the electrode surface.

3.4. Optical Absorption and Valence State of Niobium Ions

Figure 9 shows the optical absorption spectra of NbO_x deposited on a quartz glass substrate, in which those of the reagent powders of NbO, NbO₂, and Nb₂O₅ are also shown for comparison. In the absorption spectra of

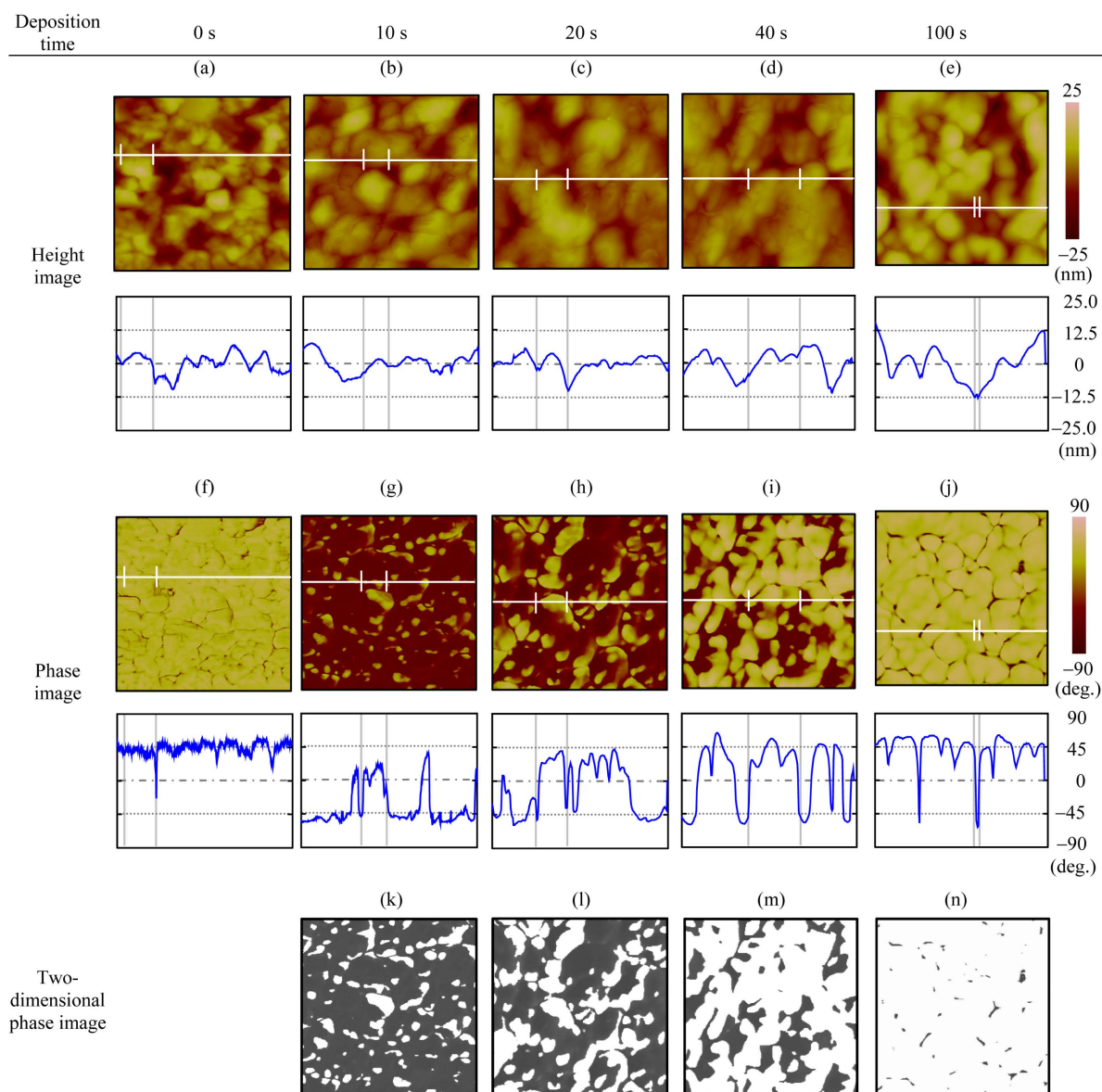


Figure 6. AFM images (height: (a)-(e), phase: (f)-(j)) of the as-prepared $\text{NbO}_x/\text{Al}/\text{glass}$ electrodes at the different NbO_x deposition time. Line scans were done at the horizontal lines drawn in the two dimensional images. Points with the phase angle $> -20^\circ$ corresponding to NbO_x deposits are indicated by white in two-dimensional phase images (k)-(n) (500 nm).

NbO_x deposits, a leading edge is commonly confirmed at ca. 2.9 eV, which is close to the absorption edge of Nb_2O_5 reagent powder. For the NbO_x deposits, a steep increase in the slope of absorption curves is also recognized at 3.5 - 3.7 eV, which is close to the band gap of 3.4 eV generally known for Nb_2O_5 . In our measurement, however, the optical band gap of Nb_2O_5 reagent powder is ca. 3.1 eV, which is smaller than the energy gap of 3.4 eV given in literatures, and it is hence suggested that the NbO_x deposits have different electronic state or atomistic structure from Nb_2O_5 crystal. Actually, no crystalline diffraction peaks are observed in XRD patterns of the NbO_x deposits, indicating that the NbO_x deposits are in amorphous state. It is supposed that the amorphous state of the NbO_x deposits is due to oxygen deficiency, and it is also expected that part of Nb ions are reduced to 4+ or 2+ from 5+. The reagent powders of crystalline NbO_2 and NbO consisting of lower valency of niobium ions show strong absorption in almost the entire region. The NbO_x deposits indicate quite different absorption spectra from NbO_2 and NbO . Therefore, it is difficult to estimate the valence state of niobium ions in the NbO_x deposits, but it is supposed that most of Nb ions are present as 5+.

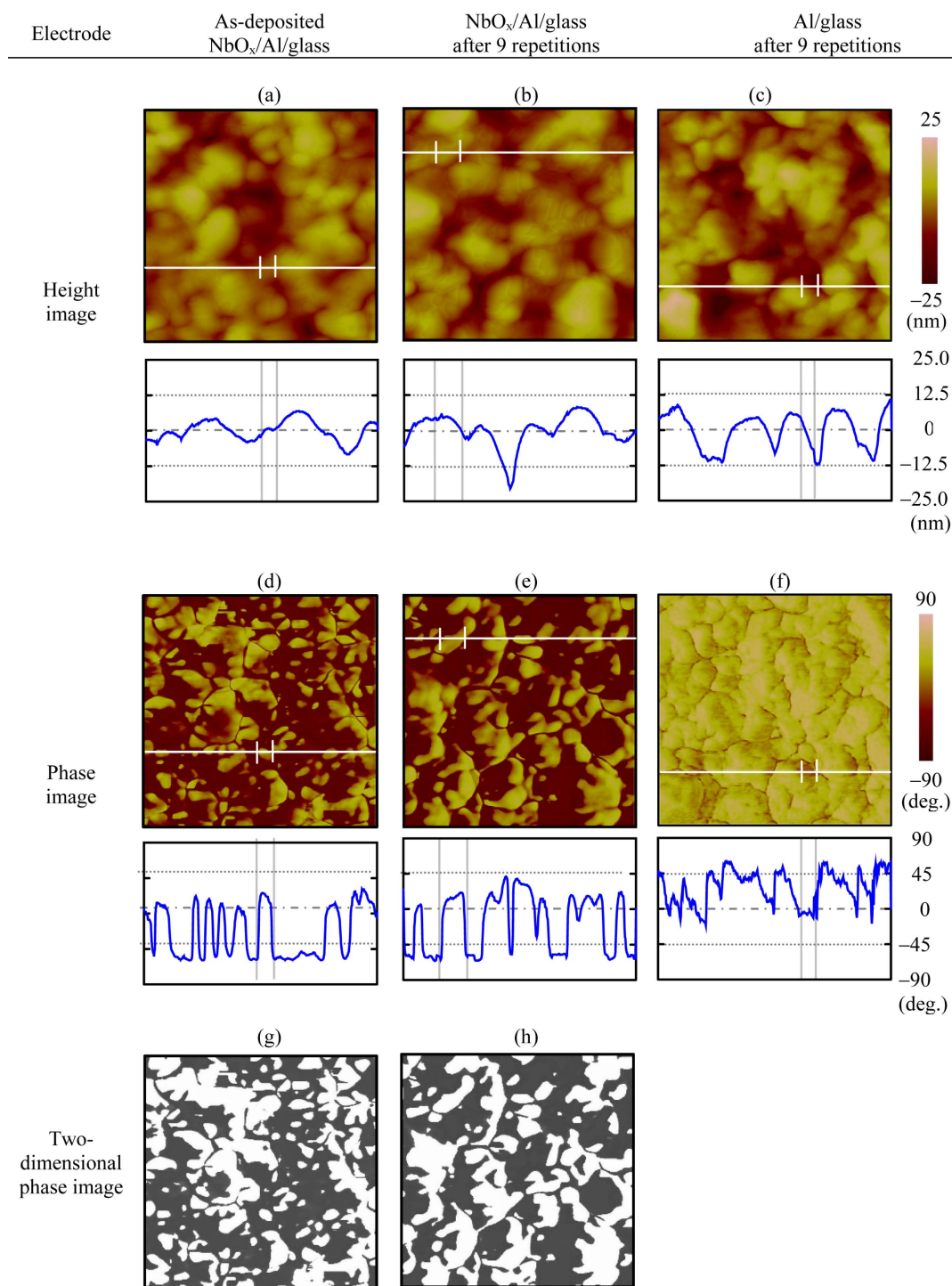


Figure 7. AFM images of NbO_x/Al/glass electrode (NbO_x deposition time = 17 s) as-deposited and after 9 repetitions of photo irradiation in the photoelectrochemical measurement (Figure 3). AFM images of Al/glass counter electrode after the photoelectrochemical measurement are also shown (500 nm).

4. Discussion

4.1. Electrochemical Reactions

As mentioned, the elution of Al and Zn from ZnO/Al/glass electrodes is observed regardless of light irradiation,

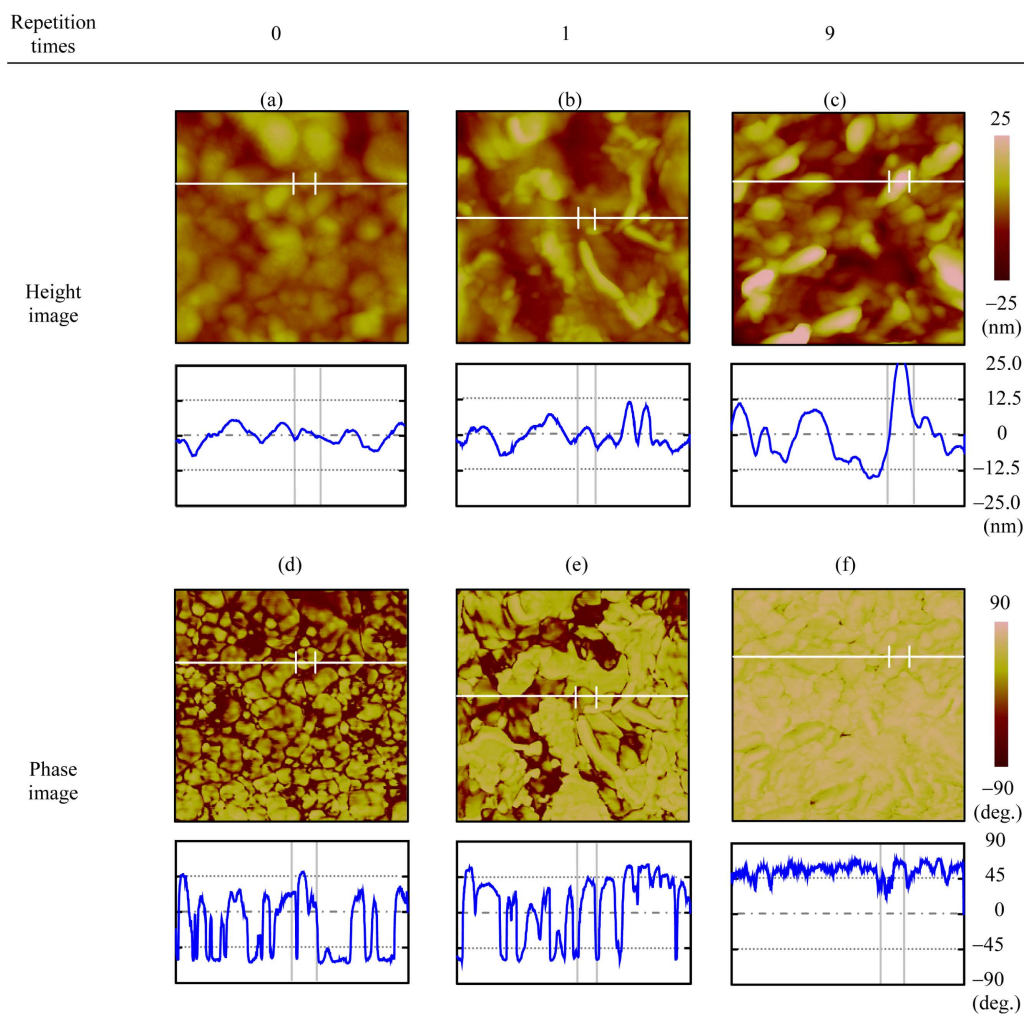


Figure 8. AFM images of the ZnO/Al/glass electrode at the ZnO deposition time of 3 s before and after repetitions of photoelectrochemical measurement. Line scans were done at the horizontal lines drawn in the two dimensional images (500 nm).

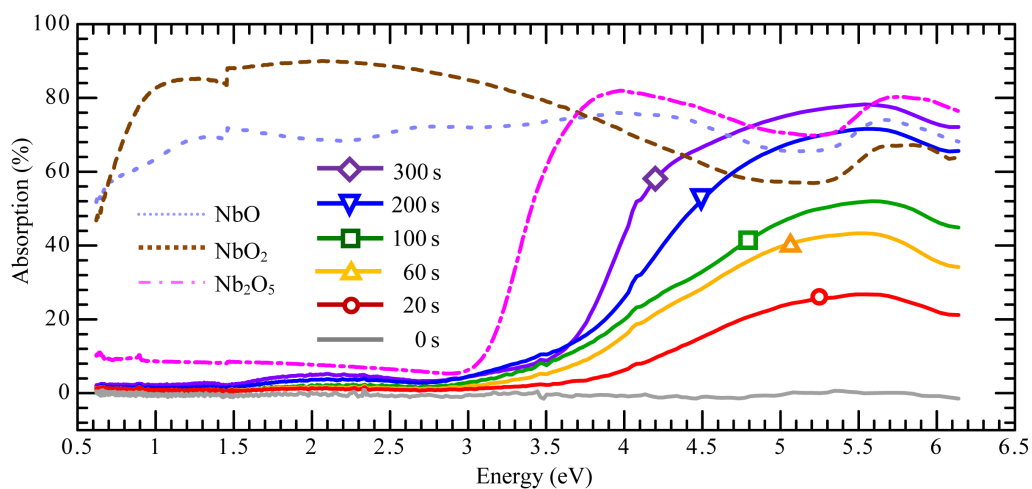


Figure 9. Absorption spectra of NbO_x deposits on a quartz glass substrate obtained by double beam transmission measurement and reagent powders of NbO, NbO₂, and Nb₂O₅ measured with an integrating sphere.

and such the elution is not recognized in $\text{NbO}_x/\text{Al}/\text{glass}$ electrodes, which are explainable by the electrochemical corrosion based on potential-pH diagrams [32]. It is known that ZnO is dissolved in acidic and alkaline water but is not soluble in neutral water [33] [34]. It is also known that metallic aluminum is easily corroded by water, and in practice, however, surface Al is oxidized to be covered with insoluble and passive Al_2O_3 skins, which prevents Al corrosion in neutral water [35] [36]. Even in neutral water, Al may be corroded by some corrosion processes, such as galvanic, crevice and pitting corrosions. In galvanic corrosion, a base metal with lower electrode potential will work as anode and corrodes in the combination with noble materials having higher electrode potential. As shown in **Table 2**, Al/glass has the lowest electrode potential among the electrode constituents. If the galvanic corrosion were predominant, Al elution from $\text{NbO}_x/\text{Al}/\text{glass}$ electrodes would be observed. However, Al elution is confirmed only in the ZnO/Al/glass electrodes, and it is hence supposed that the galvanic corrosion is not responsible for the Al elution from the ZnO/Al/glass electrodes.

Figure 10 shows that the magnified AFM images of the ZnO/Al/glass and $\text{NbO}_x/\text{Al}/\text{glass}$ electrodes at the

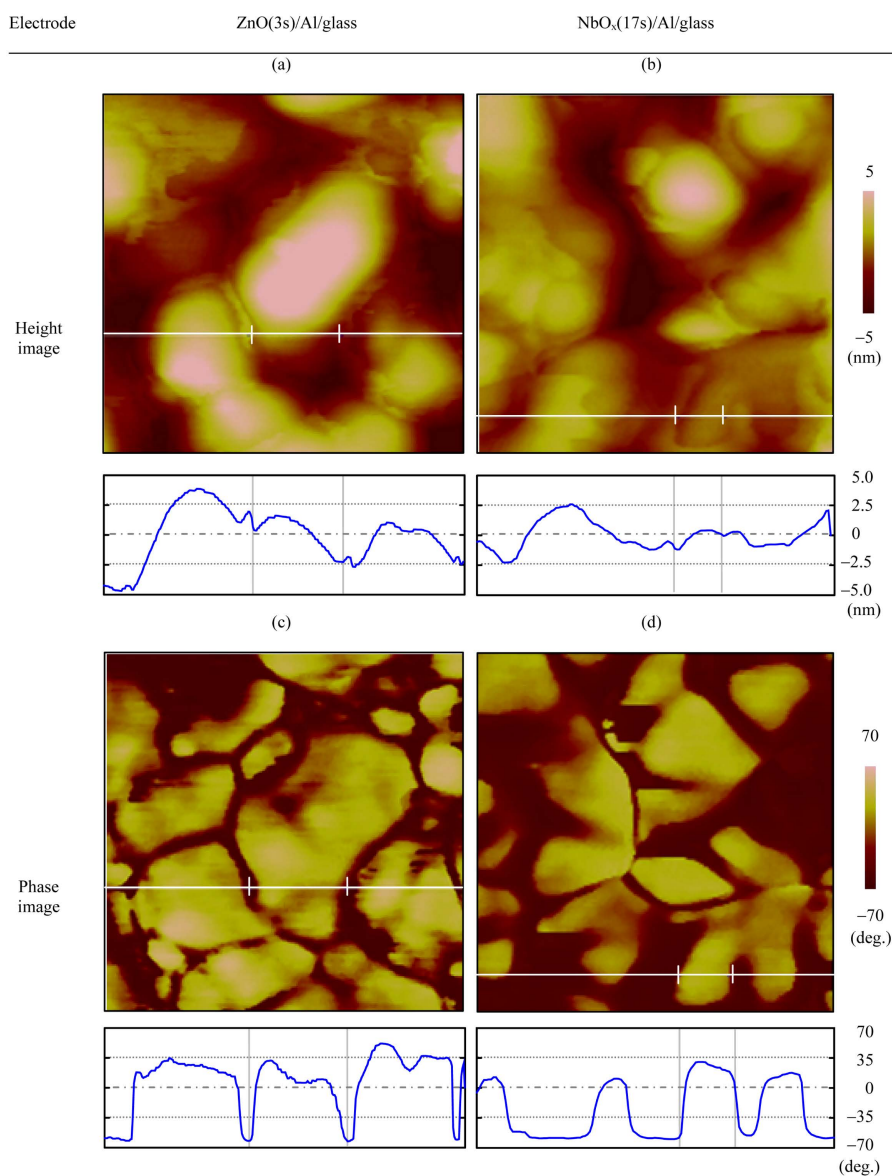


Figure 10. Magnified AFM images of the ZnO/Al/glass and $\text{NbO}_x/\text{Al}/\text{glass}$ electrodes at the deposition time of 3 and 17 s, respectively. Line scans were done at the horizontal lines drawn in the two dimensional images (150 nm).

deposition times of 3 and 17 s, respectively. Nano-dips with the depth of ca. 1 nm at brinks of nano-islands (vertical lines in **Figure 10**) are observed in both electrodes, which are probably produced by sputtering damages. At the dips in Al films, passive Al_2O_3 skins should be removed, and metallic Al might be exposed. Some of the dips should be covered with ZnO and NbO_x deposits, and therefore, pitting and/or crevice corrosions are more likely to occur at the Al/glass surface. The supposed corrosion mechanism for ZnO/Al/glass electrode is illustrated in **Figure 11**. The pitting and crevice corrosions are initiated by an anode reaction, $\text{Al} \rightarrow \text{Al}^{3+} + 3\text{e}^-$. The electrons migrate toward ZnO deposits, because ZnO has higher electrode potential than Al (**Table 2**). When oxygen is dissolved in neutral water, a cathode reaction, $\text{O}_2 + 2\text{H}_2\text{O} + 4\text{e}^- \rightarrow 4\text{OH}^-$ is expected at the surface of ZnO deposits, resulting in $\text{Al}(\text{OH})_3$ precipitation [36]. After consuming dissolved oxygen in pits and crevices, a hydrolysis reaction of Al^{3+} ions, $\text{Al}^{3+} + 3\text{H}_2\text{O} \rightarrow \text{Al}(\text{OH})_3 + 3\text{H}^+$ will be induced, and pH in the pits and crevices subsequently reduces. In acidic water in the pits and crevices promotes the corrosion of Al and dissolution of $\text{Al}(\text{OH})_3$. At the same time, ZnO deposits which cover the crevices should be also dissolved by the acidic water, $\text{ZnO} + 2\text{H}^+ \rightarrow \text{Zn}^{2+} + \text{H}_2\text{O}$ [37]. It is known that Nb_2O_5 is soluble in neutral water [38], and as shown in **Table 2**, however, $\text{NbO}_x/\text{Al}/\text{glass}$ electrodes have higher electrode potential than Al/glass substrate. It is hence supposed that NbO_x deposits are less corroded than Al films on glass. If Al films are corroded and pH in crevice water reduces, NbO_x deposits which cover the crevices should not be dissolved, because Nb ions in NbO_x deposits are almost present with valency of 5+, and Nb_2O_5 is insoluble and passive for acidic water [38]. In these ways, the elution of Al and Zn only from ZnO/Al/glass electrodes is explainable based on the pitting and/or crevice corrosions and the subsequent pH change of water in the pits and crevices. The passivation of NbO_x deposits is also described based on the potential-pH diagram.

4.2. Photoelectrochemical Reactions

As shown in **Figure 5**, the maximum power density, P_{max} is not proportional to the deposition time of NbO_x deposits, and the maximum P_{max} is obtained at the deposition time of 17 s. As shown in **Figure 9**, the optical absorption increases almost linearly with increasing the deposition time of NbO_x , and shift of the optical band gap is not observed, suggesting that the valence state and atomistic structure of NbO_x deposits remain unchanged even in the longer deposition time.

As above mentioned, during light irradiation, electrons flow from the counter electrode into the photovoltaic electrode through the external circuit, and at the same time, very small and few bubbles are formed. Moreover, Al elution from the counter electrodes is observed in the ZnO- and NbO_x -based PECs. Hence, electrochemical reactions given in Equations (1) and (2) are suggested, that is, reduction of nitrate ions and H_2 generation by reduction reactions at the photovoltaic electrodes and Al elution and O_2 generation by oxidation reactions at the counter electrode.

In the case of NbO_x deposits, the electrons consumed in the reduction reactions are probably provided from the NbO_x deposits, in which the electrons are excited into the conduction band by absorbing the irradiated light. It is also supposed that the reduction reactions occur at the interface between NbO_x deposits and electrolyte

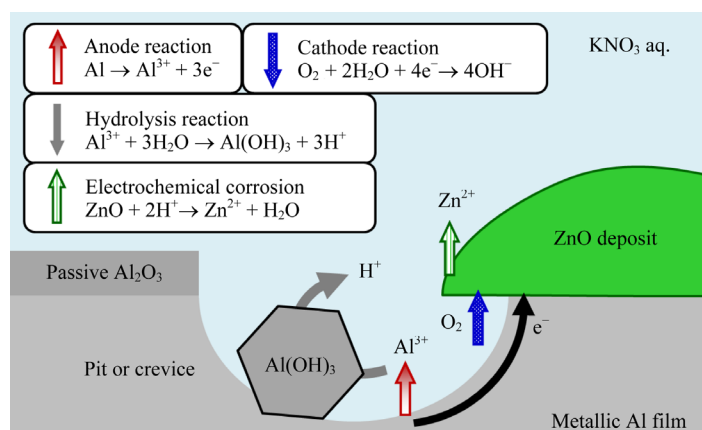


Figure 11. Electrochemical corrosion mechanism of Al and ZnO from the ZnO/Al/glass electrode in the cell of ZnO/Al/glass| KNO_3aq |Al/glass.

solution. However, the maximum power density is not proportional to the NbO_x deposition time, and it is hence suggested that the reduction reactions occur only at the restricted surface of the NbO_x deposits. It is consequently considered that most of the electrons excited by optical absorption are consumed to recombine with the holes created at the same time, and the residual holes are presumably filled with the electrons supplied from the external circuit through the Al film on the substrate electrode.

NbO_x is probably an n-type semiconductor as well as Nb_2O_5 . When a semiconductor electrode is soaked in an electrolyte solution with different electrostatic potential, a potential bending occurs in the electrode surface, which induces migrations of electrons and holes. In case of the NbO_x -based PEC, it is expected that electrons are concentrated at the surface of NbO_x deposits, and if present, holes migrate toward the underlying Al film. In the case of nano-islands, the thickness is too small to bend the surface potential, resulting in almost no potential gradient, which is similar to a flat-band state. In flat-band state, mobility and migration distance of electrons and holes are quite small, and it is hence expected that only the holes produced very near the Al film recombine with electrons which are supplied through the Al film. It is consequently supposed that the photoelectrochemical reactions proceed in the immediate vicinity of the boundary among NbO_x nano-island, Al film, and electrolyte solution.

Then, the boundary is estimated from the two-dimensional AFM phase images given in Figure 6, in which the boundary between the NbO_x deposits and the underlying Al film also means the boundary with the electrolyte solution. Figure 12 shows the boundary length obtained from an image analysis of Figure 6. For comparison, projected area of the NbO_x deposits was estimated from Figure 6, and the results are also given in Figure 12. The boundary length becomes the longest at the NbO_x deposition time of 17 s, which is consistent with the deposition time obtaining the maximum photocurrent density (J_{sc}) and power density (P_{max}) shown in Figure 5. The NbO_x projected area increases continuously with increasing the deposition time, and the slope changes at around the deposition time of 40 s, suggesting the change in growth direction of the islands from horizontal to vertical.

As shown in Figure 12(a), boundary length decreases continuously with increasing the NbO_x deposition time > 17 s. In J_{sc} and P_{max} , however, second maxima are observed at the NbO_x deposition times of 100 and 150 s, respectively (Figure 5). As mentioned, NbO_x deposits grow in the vertical direction at the deposition time > 40 s, and it is hence supposed that the thickness of NbO_x islands and films increases continuously. In these specimens, NbO_x deposits should have enough thickness to yield potential bending, from which electrons and holes generated by photo irradiation are able to migrate in the thickness direction and reach the outermost surface and innermost bottom surface of NbO_x deposits, resulting in the photoelectrochemical conversion.

Figure 13 shows the photoelectrochemical conversion mechanism proposed for the NbO_x -based PECs. In the case of nano-islands, it is supposed that the photoelectrochemical reactions in the photovoltaic electrodes take place just around the boundary, and hence most of the deposits far from the boundary should have little contribution to the electric power generation. In the case of film, it is also suggested that the photoelectrochemical conversion reactions occur at the film surface, and the reactions, however, should be restricted at part of the

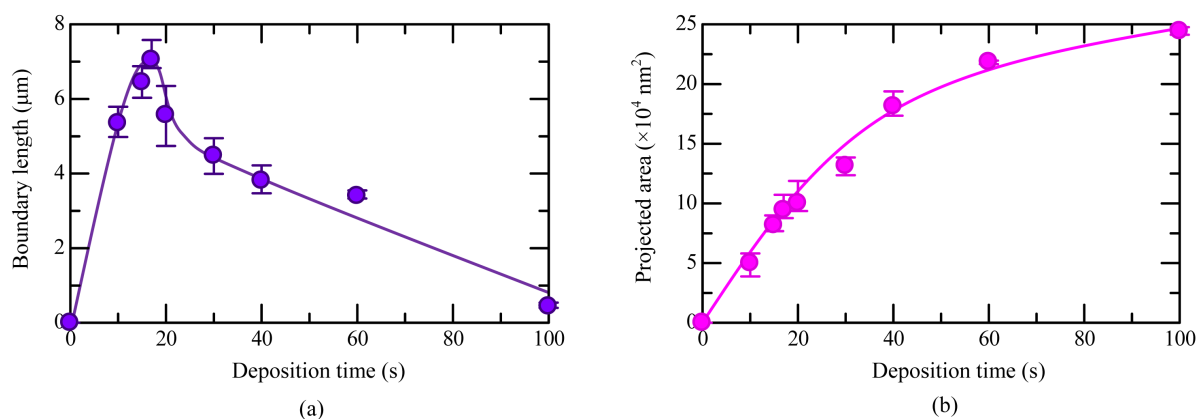


Figure 12. (a) Length of the boundary among NbO_x deposits, underlying Al film and electrolyte solution (boundary length between the white and black regions in Figure 6) and (b) projected area of NbO_x deposits (area of the white color region in Figure 6) estimated from the two-dimensional AFM phase images.

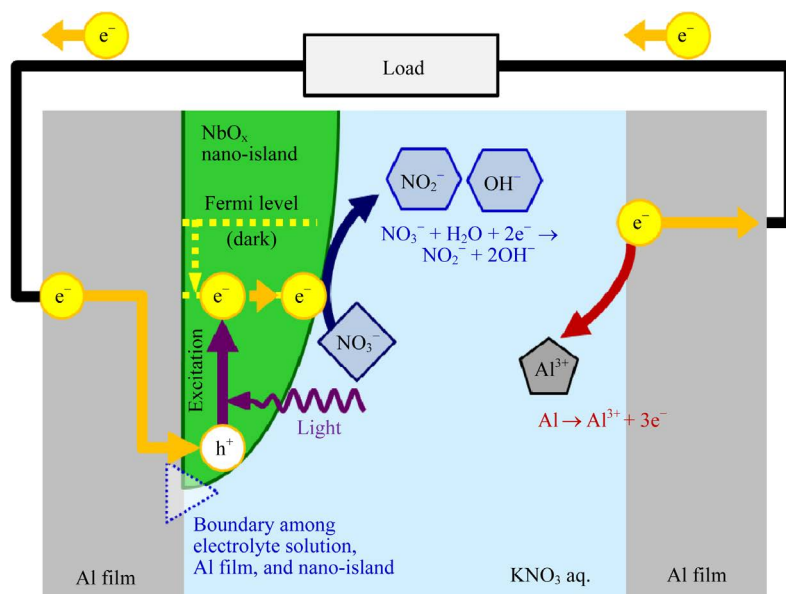


Figure 13. Photoelectrochemical conversion mechanism for the PEC consisting of NbO_x with nano-island.

surface, because the maxima in J_{sc} and P_{max} of nano-island state are larger than those of film state (Figure 5) even though the absorption of irradiated light, that is, the amount of electrons excited into conduction band increases continuously with increasing the NbO_x deposition time (Figure 9). To improve the power density, it is necessary to increase the boundary length by suppressing the growth of islands parallel to substrate to prevent the contact between the islands despite increasing the number of islands and promoting the growth of islands perpendicular to substrate to achieve the potential bending to improve the carrier mobility.

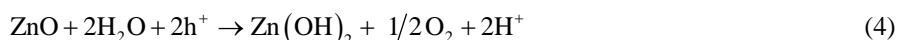
4.3. Photoelectrochemical Stability

In the case of ZnO, various photo corrosion reactions by holes have been proposed.

Han *et al.* [39]:



Rao *et al.* [40]:



Fruhwith *et al.* [37]:



A corrosion reaction, $\text{Al} + 3\text{h}^+ \rightarrow \text{Al}^{3+}$ is also assumed [12]. As above mentioned, the elution of Zn and Al from ZnO/Al/glass electrode is surely observed, and the elution rate increases during the light irradiation, which is probably due to the photo corrosion reactions concerning holes.

When combined with the results from the AFM observation (Figure 8), it is suggested that ZnO nano-islands and underlying Al film are once eluted due to the photo-induced electrochemical corrosions, and the eluted Zn^{2+} and Al^{3+} ions are promptly re-precipitated as hydroxides of $\text{Zn}(\text{OH})_2$ and $\text{Al}(\text{OH})_3$ due to the change in pH of the electrolyte solution, which is due to the OH^- forming and H^+ consuming reactions given in Equation (1). At the deposition time of 3 s, the precipitates seem to cover all the surfaces after 9th light irradiation (Figure 8(c), Figure 8(f)). It is known that $\text{Zn}(\text{OH})_2$ easily dehydrates to change into ZnO [41], and it is therefore supposed that part of the $\text{Zn}(\text{OH})_2$ precipitates change into ZnO. In case of the deposition time of 3 s, the dehydrated ZnO layer is probably thin but is enough to form potential bending so that electrons and holes can migrate between underlying Al film and electrolyte solution, resulting in photocurrent generation after repeating photo irradiation (Figure 3). As for the ZnO-based PEC at the deposition time of 17 s, the $\text{Zn}(\text{OH})_2$ insulating layer must be

thicker than the case of 3 s deposition, and hence photocurrent generation does not happen even though the ZnO layer is formed on the Zn(OH)₂ layer.

According to a potential-pH diagram of Nb system [38], Nb₂O₅ is passive and insoluble in acidic water but is soluble in neutral and alkaline water. According to Equation (1), pH of electrolyte should be increases with proceeding the photoelectrochemical reactions. Actually, slight increase in pH ~0.2 is confirmed after the photocurrent measurements. Nb⁵⁺ ions are probably dominant in NbO_x deposits, and hence NbO_x deposits should be dissolved in the electrolyte solution. However, Nb elution is not confirmed by ICP measurement. It is therefore supposed that some protection layer is formed on the surface of NbO_x deposits. According to the potential-pH diagram, NbO₂ and NbO with lower valence states are passive and insoluble at the entire pH region. In the present PECs, the NbO_x/Al/glass electrodes are negatively polarized, and electrons are concentrated at the electrode surface. It is consequently expected that some of Nb⁵⁺ ions are reduced to 4+ or lower valence state to form a highly passive layer, from which high photo corrosion resistance of NbO_x/Al/glass electrodes should be achieved.

5. Conclusions

ZnO and NbO_x were deposited on Al-coated glass substrates by an RF magnetron reactive sputtering, and photoelectrochemical cells, PECs were constructed, in which an Al/glass was used as a counter electrode and KNO₃ solution was chosen as an electrolyte. Electrochemical and photoelectrochemical properties of the PECs were evaluated.

Under the light irradiation from a solar simulator, faint and unstable photocurrent generation was seen in ZnO-based PECs. As for the NbO_x electrode, however, stable generation was successfully achieved. Very small and few bubbles were generated at both electrodes, and Al elution was found at the counter electrodes. The maximum power output was not proportional to the deposition time of NbO_x, and larger output was obtained when the NbO_x deposits were not in film, but in nano-island structures.

The photoelectrochemical properties were discussed based on the electrochemical properties. The ZnO and NbO_x electrodes had higher electrode potentials than the counter Al/glass electrode, and electron flows from the counter electrode to the ZnO or NbO_x electrodes through the external circuit were commonly confirmed. It was hence supposed that the bubbles generated during the light irradiation were H₂ at ZnO and NbO_x electrodes and O₂ at the counter Al/glass electrode. In the ZnO-based PEC, the elution of Zn and underlying Al from the ZnO electrode was observed in a dark place, and the elution rate increased during the light irradiation. After the light irradiation, precipitates on the ZnO electrode surface were found in the AFM observations. According to the potential-pH diagrams, it was suggested that the eluted Zn²⁺ and Al³⁺ ions were re-precipitated as hydroxides of Zn(OH)₂ and Al(OH)₃ on the electrode surface, which was due to the change in pH of the electrolyte solution, being resulted from the OH⁻ generating and H⁺ consuming reactions. During the repetition of photo irradiation, the Zn(OH)₂ precipitates changed into thin ZnO layer, resulting in photocurrent generation. At the NbO_x electrode, elution was observed neither in a dark place nor during the light irradiation, and quite little change was observed on the NbO_x electrode surface. From the optical absorption spectra, it was suggested that Nb ions in NbO_x deposits were almost present as Nb⁵⁺, but they had different electronic state or atomistic structure from Nb₂O₅ crystal. Furthermore, it was also suggested that the electronic state and atomistic structure of NbO_x deposits were unchanged and independent of the deposition time. The maximum power output was correlated not with the deposition time but with the length of the boundary between the NbO_x nano-islands and the underlying Al film. Second maximum in power output was also obtained at the longer NbO_x deposition time, where thin film of NbO_x deposits was formed. Larger power generation was obtained with the NbO_x deposits with nano-island structure.

Based on the experimental findings, the following photoelectrochemical reaction mechanism was suggested: due to the light irradiation, electrons in the NbO_x deposits were excited into the conduction band, and were used in the reduction of NO₃⁻ ions and H₂ gas generation. The holes were filled with the electrons supplied from the Al/glass substrate through the external circuit. In the case of NbO_x deposits with nano-island structure, it was finally concluded that the photoelectrochemical reactions proceeded in the vicinity of the boundary among the nano-islands, substrate and electrolyte solution, which was a distinctive characteristic derived from the electrodes with nano-island structure. Nano-island was expected as a novel electrode structure in PECs, which might provide higher efficiency in photoelectrochemical conversion by the improvements in geometry designs of nano-islands, choice of materials and deposition conditions.

References

- [1] Guillemin, N., Heurtault, B.J.B., Geerligs, L.J. and Weeber, A.W. (2011) Development towards 20% Efficient Si MWT Solar Cells for Low-Cost Industrial Production. *Energy Procedia*, **8**, 9-16.
<http://dx.doi.org/10.1016/j.egypro.2011.06.094>
- [2] De Wolf, S., Duerinckx, F., Agostinelli, G. and Beaucarne, G. (2006) Low-Cost Rear Side Floating Junction Solar-Cell Issues on mc-Si. *Solar Energy Materials and Solar Cells*, **90**, 3431-3437.
<http://dx.doi.org/10.1016/j.solmat.2006.02.035>
- [3] Huang, J.Y., Lin, C.Y., Shen, C.H., Shieh, J.M. and Dai, B.T. (2012) Low Cost High-Efficiency Amorphous Silicon Solar Cells with Improved Light-Soaking Stability. *Solar Energy Materials and Solar Cells*, **98**, 277-282.
<http://dx.doi.org/10.1016/j.solmat.2011.11.023>
- [4] Terakawa, A. (2013) Review of Thin-Film Silicon Deposition Techniques for High-Efficiency Solar Cells Developed at Panasonic/Sanyo. *Solar Energy Materials and Solar Cells*, **119**, 204-208.
<http://dx.doi.org/10.1016/j.solmat.2013.06.044>
- [5] Chaudhari, V.A. and Solanki, C.S. (2010) A Novel Two Step Metallization of Ni/Cu for Low Concentrator c-Si Solar Cells. *Solar Energy Materials and Solar Cells*, **94**, 2094-2101. <http://dx.doi.org/10.1016/j.solmat.2010.06.032>
- [6] Chu, L.K., Yen, C.W. and Sayed, M.A.E. (2010) Bacteriorhodopsin-Based Photo-Electrochemical Cell. *Biosensors and Bioelectronics*, **26**, 620-626. <http://dx.doi.org/10.1016/j.bios.2010.07.013>
- [7] Barote, M.A., Kamble, S.S., Deshmukh, L.P. and Masumdar, E.U. (2013) Photo-Electrochemical Performance of $Cd_{1-x}Pb_xS$ ($0 \leq x \leq 1$) Thin Films. *Ceramics International*, **39**, 1463-1467.
<http://dx.doi.org/10.1016/j.ceramint.2012.07.090>
- [8] Tseng, C.J., Wang, C.H. and Cheng, K.W. (2012) Photoelectrochemical Performance of Gallium-Doped $AgInS_2$ Photoelectrodes Prepared by Electrodeposition Process. *Solar Energy Materials and Solar Cells*, **96**, 33-42.
<http://dx.doi.org/10.1016/j.solmat.2011.09.010>
- [9] Trunk, M., Sobas, A.G., Venkatachalapathy, V., Zhang, T., Galeckas, A. and Kuznetsov, A.Y. (2012) Testing ZnO Based Photoanodes for PEC Applications. *Energy Procedia*, **22**, 101-107.
<http://dx.doi.org/10.1016/j.egypro.2012.05.221>
- [10] Jacobsson, T.J., Björkman, C.P., Edoff, M. and Edvinsson, T. (2013) $CuIn_xGa_{1-x}Se_2$ as an Efficient Photocathode for Solar Hydrogen Generation. *International Journal of Hydrogen Energy*, **38**, 15027-15035.
<http://dx.doi.org/10.1016/j.ijhydene.2013.09.094>
- [11] Fujishima, A. and Honda, K. (1972) Electrochemical Photolysis of Water at a Semiconductor Electrode. *Nature*, **238**, 37-38. <http://dx.doi.org/10.1038/238037a0>
- [12] Imajo, T., Okano, H. and Maeda, A. (2008) Photocatalytic Lithography Using Zinc Oxide Nanoislands. *Japanese Journal of Applied Physics*, **47**, 2330. <http://dx.doi.org/10.1143/JJAP.47.2330>
- [13] Prado, A.G.S., Bolzon, L.B., Pedroso, C.P., Moura, A.O. and Costa, L.L. (2008) Nb_2O_5 as Efficient and Recyclable Photocatalyst for Indigo Carmine Degradation. *Applied Catalysis B: Environmental*, **82**, 219-224.
<http://dx.doi.org/10.1016/j.apcatb.2008.01.024>
- [14] Roza, L., Rahman, M.Y.A., Umar, A.A. and Salleh, M.M. (2015) Direct Growth of Oriented ZnO Nanotubes by Self-Selective Etching at Lower Temperature for Photo-Electrochemical (PEC) Solar Cell Application. *Journal of Alloys and Compounds*, **618**, 153-158. <http://dx.doi.org/10.1016/j.jallcom.2014.08.113>
- [15] Suzuki, S., Teshima, K., Ishizaki, T., Lee, S.H., Yubuta, K., Shishido, T. and Oishi, S. (2011) Unique Three-Dimensional Nano-/Micro-Textured Surfaces Consisting of Highly Crystalline Nb_2O_5 Nanotubes. *Journal of Crystal Growth*, **318**, 1095-1100. <http://dx.doi.org/10.1016/j.jcrysgro.2010.11.129>
- [16] Nayeri, F.D., Soleimani, E.A. and Salehi, F. (2013) Synthesis and Characterization of ZnO Nanowires Grown on Different Seed Layers: The Application for Dye-Sensitized Solar Cells. *Renewable Energy*, **60**, 246-255.
<http://dx.doi.org/10.1016/j.renene.2013.05.006>
- [17] Lin, Y., Yang, Y.J. and Hsu, C.C. (2011) Synthesis of Niobium Oxide Nanowires Using an Atmospheric Pressure Plasma Jet. *Thin Solid Films*, **519**, 3043-3049. <http://dx.doi.org/10.1016/j.tsf.2010.12.024>
- [18] Ye, N., Qi, J., Qi, Z., Zhang, X., Yang, Y., Liu, J. and Zhang, Y. (2010) Improvement of the Performance of Dye-Sensitized Solar Cells Using Sn-Doped ZnO Nanoparticles. *Journal of Power Sources*, **195**, 5806-5809.
<http://dx.doi.org/10.1016/j.jpowsour.2010.03.036>
- [19] Méndez, S.M., Henríquez, Y., Domínguez, O., D'Ornelas, L. and Krentzien, H. (2006) Catalytic Properties of Silica Supported Titanium, Vanadium and Niobium Oxide Nanoparticles towards the Oxidation of Saturated and Unsaturated Hydrocarbons. *Journal of Molecular Catalysis A: Chemical*, **252**, 226-234.
<http://dx.doi.org/10.1016/j.molcata.2006.02.041>

- [20] Kang, Z., Gu, Y., Yan, X., Bai, Z., Liu, Y., Liu, S., Zhang, X., Zhang, Z., Zhang, X. and Zhang, Y. (2015) Enhanced Photoelectrochemical Property of ZnO Nanorods Array Synthesized on Reduced Graphene Oxide for Self-Powered Biosensing Application. *Biosensors and Bioelectronics*, **64**, 499-504. <http://dx.doi.org/10.1016/j.bios.2014.09.055>
- [21] Wen, H., Liu, Z., Wang, J., Yang, Q., Li, Y. and Yu, J. (2011) Facile Synthesis of Nb₂O₅ Nanorod Array Films and Their Electrochemical Properties. *Applied Surface Science*, **257**, 10084-10088. <http://dx.doi.org/10.1016/j.apsusc.2011.07.001>
- [22] Kou, H., Zhang, X., Du, Y., Ye, W., Lin, S. and Wang, C. (2011) Electrochemical Synthesis of ZnO Nanoflowers and Nanosheets on Porous Si as Photoelectric Materials. *Applied Surface Science*, **257**, 4643-4649. <http://dx.doi.org/10.1016/j.apsusc.2010.12.108>
- [23] Choi, B., Myung, N. and Rajeshwar, K. (2007) Double Template Electrosynthesis of ZnO Nanodot Array. *Electrochemistry Communications*, **9**, 1592-1595. <http://dx.doi.org/10.1016/j.elecom.2007.02.025>
- [24] Qi, S., Zuo, R., Liu, Y. and Wang, Y. (2013) Synthesis and Photocatalytic Activity of Electrospun Niobium Oxide Nanofibers. *Materials Research Bulletin*, **48**, 1213-1217. <http://dx.doi.org/10.1016/j.materresbull.2012.11.074>
- [25] Bonakdarpour, A., Tucker, R.T., Fleischauer, M.D., Beckers, N.A., Brett, M.J. and Wilkinson, D.P. (2012) Nanopillar Niobium Oxides as Support Structures for Oxygen Reduction Electrocatalysts. *Electrochimica Acta*, **85**, 492-500. <http://dx.doi.org/10.1016/j.electacta.2012.08.005>
- [26] Hayashi, Y., Arita, M., Koga, K. and Masuda, M. (1995) Photo-Electrochemical Properties of Hydrogen in Anodically Oxidized Niobium. *Journal of Alloys and Compounds*, **231**, 702-705. [http://dx.doi.org/10.1016/0925-8388\(95\)01756-9](http://dx.doi.org/10.1016/0925-8388(95)01756-9)
- [27] Sugisaki, N., Niizuma, K. and Ikawa, H. (2010) Photocatalytic Effect of Niobium Oxide Film by RF Magnetron Sputtering Method. College of Industrial Technology, Nihon University Lecture Meeting.
- [28] Lide, D.R. (2001) CRC Handbook of Chemistry and Physics. 82nd Edition, CRC Press, Boca Raton.
- [29] Asano, T., Kubo, T. and Nishikitani, Y. (2005) Short-Circuit Current Density Behavior of Dye-Sensitized Solar Cells. *Japanese Journal of Applied Physics*, **44**, 6776-6780. <http://dx.doi.org/10.1143/JJAP.44.6776>
- [30] Kim, J.H. and Ahn, K.S. (2010) Tri-Branched Tri-Anchoring Organic Dye for Visible Light-Responsive Dye-Sensitized Photoelectrochemical Water-Splitting Cells. *Japanese Journal of Applied Physics*, **49**, Article ID: 060219. <http://dx.doi.org/10.1143/JJAP.49.060219>
- [31] Onodera, M., Nagumo, R., Miura, R., Suzuki, A., Tsuboi, H., Hatakeyama, N., Endou, A., Takada, H., Kubo, M. and Miyamoto, A. (2011) Multiscale Simulation of Dye-Sensitized Solar Cells Considering Schottky Barrier Effect at Photoelectrode. *Japanese Journal of Applied Physics*, **50**, Article ID: 04DP06. <http://dx.doi.org/10.1143/JJAP.50.04DP06>
- [32] Pourbaix, M. (1966) Atlas of Electrochemical Equilibria in Aqueous Solutions. Pergamon Press, Oxford.
- [33] Yagi, S., Kondo, Y., Satake, Y., Ashida, A. and Fujimura, N. (2012) Local pH Control by Electrolysis for ZnO Epitaxial Deposition on a Pt Cathode. *Electrochimica Acta*, **62**, 348-353. <http://dx.doi.org/10.1016/j.electacta.2011.12.059>
- [34] Han, Y., Chen, Z., Tong, L., Yang, L., Shen, J., Wang, B., Liu, Y., Liu, Y. and Chen, Q. (2013) Reduction of N-Nitrosodimethylamine with Zero-Valent Zinc. *Water Research*, **47**, 216-224. <http://dx.doi.org/10.1016/j.watres.2012.09.043>
- [35] Wranglén, G. (1985) An Introduction to Corrosion and Protection of Metals. Chapman & Hall, London. <http://dx.doi.org/10.1007/978-94-009-4850-1>
- [36] Kojima, Y. (2011) Electrochemical Analysis for Corrosion Behavior of Aluminum, Keikinzo. *Journal of Japan Institute of Light Metals*, **61**, 167. (In Japanese).
- [37] Fruhwirth, O., Herzog, G.W. and Poullos, J. (1985) Dark Dissolution and Photodissolution of ZnO. *Surface Technology*, **24**, 293-300. [http://dx.doi.org/10.1016/0376-4583\(85\)90079-2](http://dx.doi.org/10.1016/0376-4583(85)90079-2)
- [38] Asselin, E., Ahmed, T.M. and Alfantazi, A. (2007) Corrosion of Niobium in Sulphuric and Hydrochloric Acid Solutions at 75 and 95 °C. *Corrosion Science*, **49**, 694-710. <http://dx.doi.org/10.1016/j.corsci.2006.05.028>
- [39] Han, J., Qiu, W. and Gao, W. (2010) Potential Dissolution and Photo-Dissolution of ZnO Thin Films. *Journal of Hazardous Materials*, **178**, 115-122. <http://dx.doi.org/10.1016/j.jhazmat.2010.01.050>
- [40] Rao, M.V., Rajeshwar, K., Pal Verneker, V.R. and Du Bow, J. (1980) Photosynthetic Production of H₂ and H₂O₂ on Semiconducting Oxide Grains in Aqueous Solutions. *The Journal of Physical Chemistry*, **84**, 1987-1991. <http://dx.doi.org/10.1021/j100452a023>
- [41] Izaki, M. and Omi, T. (1996) Electrolyte Optimization for Cathodic Growth of Zinc Oxide Films. *Journal of The Electrochemical Society*, **143**, L53-L55. <http://dx.doi.org/10.1149/1.1836529>